Pergamon

Journal of Structural Geology, Vol. 16, No. 10, pp. 1403 to 1416, 1994

0191-8141/94 $7.00 + 0.00

0191-8141(94)E0024-S

Volume loss and tectonic flattening strain in granitic mylonites from the Blue Ridge province, central Appalachians

CHRISTOPHER M. BAILEY, CAROL SIMPSON and DECLAN G. DE PAOR*

Department of Earth and Planetary Sciences, The Johns Hopkins University, Baltimore, MD 21218, U.S.A.

(*Received* 21 *July* 1993; *accepted in revised form* 10 *January* 1994)

Abstract—Granitic mylonites from the Blue Ridge province in the central Appalachians demonstrate the contribution of various deformation mechanisms to the strain geometry that developed during greenschist facies deformation in thrust-related shear zones. Strain accumulated through cataclasis in feldspar, crystal plastic processes in quartz, and a significant contribution of pressure solution in both feldspar and quartz. Strain analysis was performed using R_f/ϕ_f techniques on quartz grain shapes and by measuring stretched and boudinaged feldspars. Petrographic and geochemical evidence indicates that deformation ranged from isovolumetric to upwards of 60% bulk-rock volume loss. Quartz and feldspar strain values plot within the field of apparent flattening. Feldspars in both *XZ* and *YZ* sections are boudinaged and separated by transverse veins and record a true tectonic flattening strain. Strain data indicate that the bulk deformation path in shear zones throughout the Blue Ridge province significantly deviated from plane strain.

INTRODUCTION

DEFORMATION in orogenic regions is often assumed to follow a bulk plane strain deformation path (e.g. Sanderson 1976). Most section balancing techniques necessarily assume bulk plane strain, in which material moves neither into nor out of the plane of section (Dahlstrom 1969, Boyer & Elliott 1982). However, few quantitative studies have been conducted over sufficiently large areas to evaluate this assumption (see, however, Cloos 1947, 1971, Ramsay & Huber 1983, figs. 11.8–10). The strain recorded in ductile shear zones formed at mid-crustal depths is commonly modelled assuming plane strain and inhomogeneous simple shear (Ramsay 1967). Field data support the assertion that shear zone deformation is usually strongly non-coaxial (Berthé *et al.* 1979, Davis 1980, Simpson 1983, Lister & Snoke 1984, Hanmer & Passchier 1992), but strain measurements from several shear zones indicate that apparent flattening strains are also abundant (Coward 1976, Mitra 1979, O'Hara 1990).

In any test for deviation from plane strain it is necessary to account for possible volume changes. With volume loss, the strain ellipsoid for a plane strain deformation plots in the field of apparent flattening on a Flinn diagram (Ramsay & Wood 1973). Sedimentary strata undergo compaction and volume loss during burial. If followed by loading during thrust emplacement these rocks may continue to follow an oblate deformation path, but if followed by a wrench-oriented deformation they may experience prolate strain (Ramsay & Wood 1973, Sanderson 1976). Crystalline rocks do not undergo compaction as do sediments, and they generally lack strain markers. Nevertheless, significant bulk-rock volume loss has been recorded from mylonitic crystalline rocks by O'Hara (1990) who suggested that high strain zones may localize on solution zones and that volume loss might be the rule rather than the exception. Therefore, even in crystalline rocks it is necessary to quantify volume change before an accurate evaluation of true tectonic vs apparent flattening strain is possible.

This study examines the contribution of crystal plasticity, cataclasis, and solution transfer to the deformation of granitic rocks in greenschist facies shear zones in the Virginia Blue Ridge province of the central Appalachians. Traditional strain analysis techniques are used in a new way to examine the strain geometry of quartz and feldspar grains. Whole-rock and trace element geochemical evidence indicates that volume loss occurred in some samples during deformation, but true tectonic flattening strains are also recorded.

GEOLOGIC SETTING

The Blue Ridge province is a narrow belt of predominantly Precambrian rock that separates the thin-skinned Valley and Ridge fold and thrust belt to the northwest from the Piedmont province to the southeast (Fig. 1). In northern and central Virginia, the Blue Ridge forms an anticlinorium with middle and late Proterozoic crystalline rock in its core and late Proterozoic metasedimentary and metavolcanic rock on its flanks. Seismic reflection profiles indicate that the Blue Ridge is allochthonous and has been thrust NW-ward over Paleozoic sedimentary rock of the Valley and Ridge (Harris *et al.* 1982, Evans 1989).

Middle Proterozoic basement in the Virginia Blue Ridge can be divided into layered gneiss and metaigneous rock. Radiometric ages for these rocks range from 1870 to 900 Ma (Sinha & Bartholomew 1984); layered gneisses are generally older than metaigneous

*Present Address: Department of Geology, George Washington University, Washington, DC 20052, U.S.A.

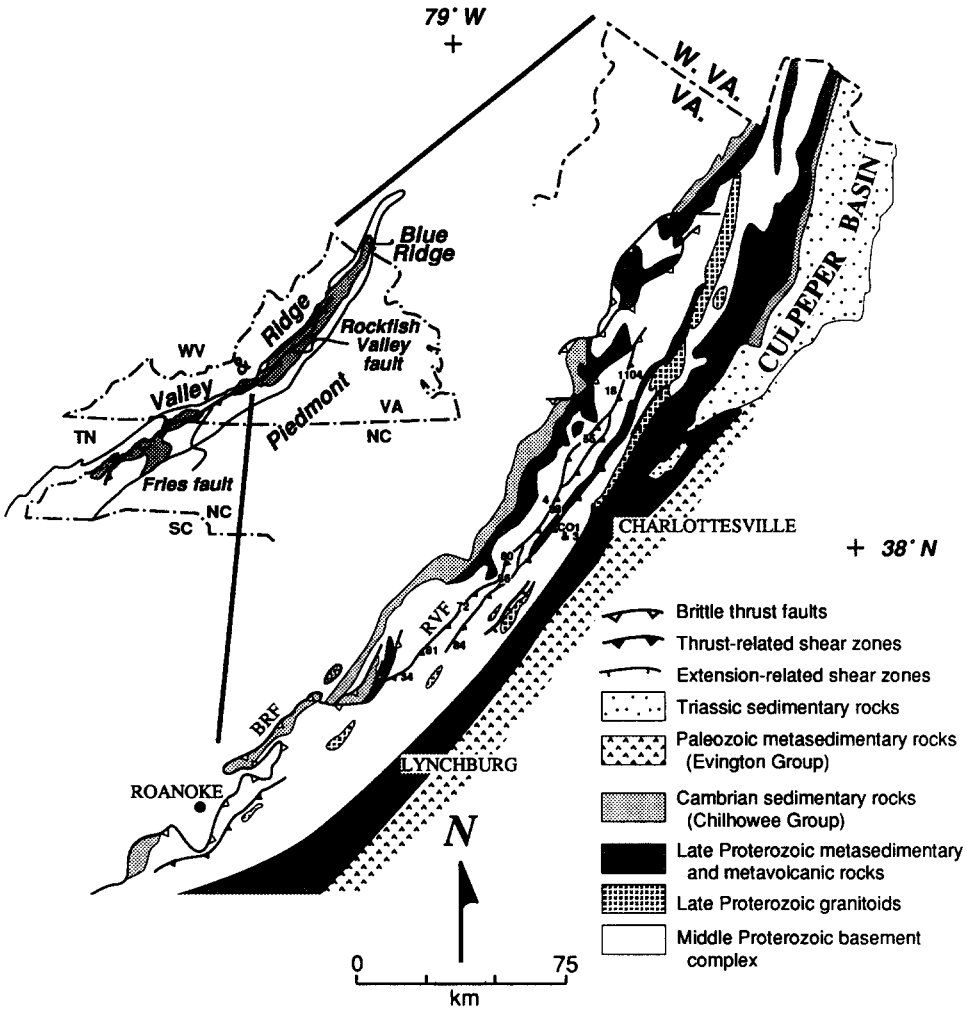

Fig. 1. Generalized geologic map of the Blue Ridge province in the central and southern Appalachians. Shaded region of small map represents Proterozoic basement granitoids. RVF—Rockfish Valley fault zone. BRF—Blue Ridge fault. Numbers on large map are sample localities.

rocks. Late Proterozoic peralkaline to metaluminous granitoids (730–650 Ma; Herz & Force 1987, Tollo & Aleinokoff 1992) intrude the older crystalline rock and are thought to be associated with pre-Iapetus rifting of eastern Laurentia (Rankin 1975, Rankin *et al.* 1989).

The Proterozoic crystalline rock in the Virginia section of the Blue Ridge province was involved in three temporally and kinematically distinct deformation episodes (Bailey & Simpson 1993). The Grenville event (approximately 1000 Ma) was a high grade deformation, whose fabrics are restricted to the older layered gneisses. A younger deformation, characterized by low-strain coaxial fabrics and high strain extensional shear zones affected much of the crystalline rocks and is thought to be associated with late Proterozoic continental rifting (see also Simpson & Kalaghan 1989). The youngest deformation event involved Paleozoic thrusting of the crystalline rock and is characterized by anastomosing shear zones that record large non-coaxial strains under greenschist facies conditions (Bailey & Simpson 1993). One of these thrust zones, the regionally extensive Rockfish Valley-Fries fault system, is a 1–3 km thick zone of protomylonite, mylonite, and ultramylonite that can be traced discontinuously from northern Virginia to central North Carolina (Fig. 1). Thrust displacement increases towards the southwest: in central and northern Virginia, Proterozoic basement comprises both hangingwall and footwall, but within the Fries fault portion, basement and cover are involved in the thrusting. We examined mylonitic rocks from the Rockfish Valley fault zone which have experienced only one episode of contractional deformation during the Paleozoic.

ROCKFISH VALLEY FAULT ZONE

Mesostructures

The protolith for Paleozoic thrust-related shear zones in the central Appalachians is quite variable and we limited our study to middle Proterozoic metaigneous rock of granitoid composition, which generally contains no discernible fabric other than the Paleozoic foliation. Middle Proterozoic biotite-rich granites, leucogranites, and charnockites are typically coarse-grained, equigranular to porphyritic, and massive away from high strain zones. The rocks range in composition from

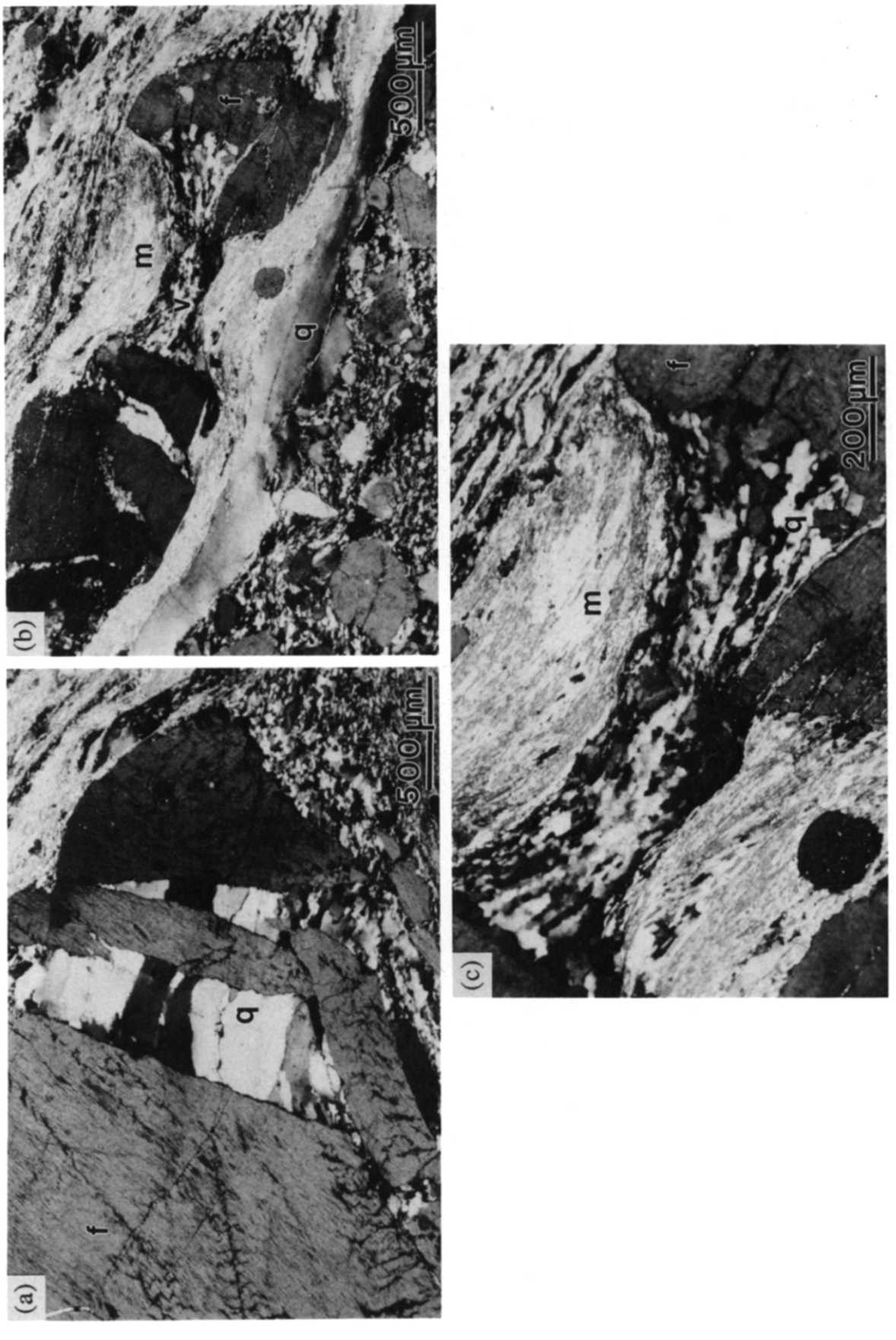

Fig. 2. Photomicrographs of XZ section from protomylonites and mylonites. Crossed polarized light. (a) Quartz-filled q cracks in alkali feldspar f at early stages of cataclasis. Note face controlled orientation of quartz fibres. (specimen BR4). (b) Boudinaged feldspar fragments f separated by quartz-filled transverse vein v with bow-tie morphology. Muscovite m mantles feldspar and quartz vein fill. Note monocrystalline quartz ribbon q with large aspect ratio. (specimen BR4). (c) Close-up of transverse vein with bow-tie morphology. Thinnest portion of vein occurs at the center, and vein thickens towards feldspar. Quartz fibres close to vein wall are not recrystallized. Quartz q, feldspar f and muscovite m. (specimen BR4).

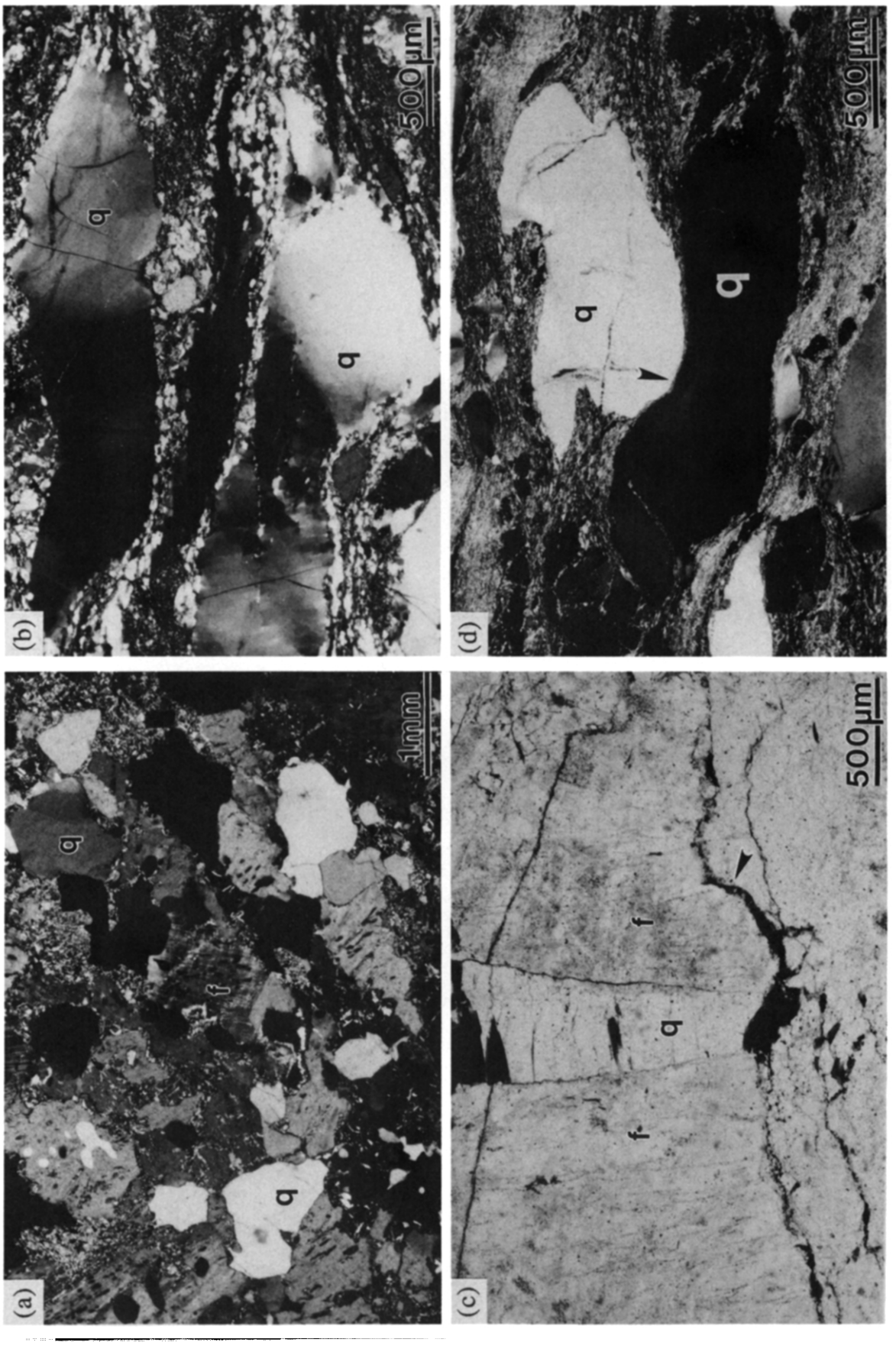

Fig. 3. Photomicrographs of *XZ* sections of protomylonites and mylonites. (a) Granitic protolith with bleb-like quartz q and undeformed feldspars f. Note no preferred grain shape orientation is visible (specimen BR57). (b) Deformed quartz lenses q with undulatory extinction and subgrain development (specimen BR18). (c) Undulatory seam of Fe-oxides (arrow) cutting alkali feldspar f grains and quartz vein filling q in fracture. Fracture opened parallel to the *X*-direction. Residue seam generally perpendicular to the *Z*-direction (specimen BR34). (d) Quartz–quartz q grain contact (arrow). Indented nature of contact suggestive of dissolution along grain boundaries (specimen BR4). (a), (b) & (d) crossed polarized light; (c) plane light.

quartz monozonites to alkali-feldspar granites and contain 15–35% quartz, 15–45% alkali feldspar, 5–25% plagioclase (An_{5-50}), and 3–20% mafic minerals. Biotite is the most abundant mafic phase, but orthopyroxene is common although slightly altered to uralitic hornblende and biotite in the charnockites. Accessory phases include epidote, sphene, ilmenite, muscovite, garnet, zircon and apatite.

Strain within shear zones is extremely variable and the transition from undeformed granite to mylonite and ultramylonite is commonly observable in outcrop, permitting comparison of protolith and its deformed equivalent. Porphyroclastic mylonites with conspicuous asymmetric kinematic indicators are abundant in shear zones. Biotite-rich mylonites are derived from biotite-bearing granitoids, while muscovite-rich and chlorite-bearing mylonites are generally derived from leucocratic alkali feldspar granites and charnockites. In hand sample, the foliation is delineated by oriented phyllosilicates, quartz lenses and ribbons, and disaggregated feldspars. The mylonitic foliation in the Rockfish Valley fault zone strikes between 020° and 055° and dips moderately to the southeast. A down-dip mineral stretching lineation defined by elongate quartz, mica, and boudinaged feldspar trains is common, but not always present.

Microstructures

At low strains, alkali and plagioclase feldspar undergo brittle fracture. These fractures are typically wedge-shaped, intragranular cracks that are filled with face-controlled quartz fibres (Fig. 2a) of similar lattice orientations. Less commonly, cracks are filled with fibrous biotite, muscovite and chlorite. Larger fractures with planar sides cross cut entire feldspar porphyroclasts, but rarely cut multiple grains. Quartz fibres are generally parallel to the foliation and lineation. Not all fractures opened parallel to the foliation and most of the oblique fractures are parallel to (010) and (100) cleavage planes in feldspar grains. Fractures oriented at large angles to the foliation generally display shear offset and are coated with chlorite, quartz and fibrous white mica.

In cracks that have opened by at least 200–400 μm, quartz fibres have generally undergone dynamic recrystallization. Strain-free recrystallized grains (50–200 μm diameter) occur as a mosaic mantling the inner edge (towards the center of the vein) of strained quartz fibres which themselves contain (50–100 μm diameter) subgrains. A transition from unstrained quartz fibres at the fracture edge to strained fibres and recrystallized strain-free mosaics at the vein center is commonly observed. At advanced stages of deformation, the feldspar fragments become widely separated along the foliation plane. Boudinaged feldspar pieces are separated by rod- or ribbon-like transverse veins (Fig. 2b) (e.g. Holmquist 1931, De Paor *et al.* 1991). Within transverse veins, recrystallization of quartz fibres is complete except close to the feldspar face where newly precipitated quartz fibres occur (Fig. 2c). Transverse veins are thickest at their margins and thinnest near their center (bow-tie shaped, Fig. 2b).

Alkali and to a lesser extent plagioclase feldspars are commonly mantled by selvages of fine-grained muscovite. Muscovite rims on alkali feldspar occur predominantly along grain boundaries perpendicular to the foliation, whereas quartz-filled veins parallel the foliation (Fig. 2b). Fine-grained biotite and granular epidote also mantle fractured feldspars in some samples. In highly extended feldspar trains, some fragments are ovoid and completely mantled by muscovite, but angular fragments of feldspar attached to quartz veins are more typical. Both unfractured feldspars and highly extended feldspar boudin trains occur in protomylonites and mylonites. In protomylonites, unfractured to weakly fractured feldspars are more common while in mylonites feldspar boudin trains are abundant. Feldspars are completely disaggregated in ultramylonites and generally completely mantled by fine-grained mica.

In the protolith, original igneous quartz grains are equidimensional or irregular fillings in interstices between feldspars (Fig. 3a). Protomylonites have a weak foliation and quartz grains are lensoidal with a strong preferred grain shape orientation. Quartz lenticles exhibit undulatory extinction, subgrain development, core and mantle structures, and deformation bands (Fig. 3b). Monocrystalline quartz ribbons, with axial ratios up to 15:1, are common (Fig. 2b). These ribbons display undulose extinction and have very low interference colors in thin sections parallel to the lineation and perpendicular to the foliation. Narrow ($<50\,\mu$m) deformation bands, oblique to the long dimension of the strain-free grains are also present. Less common are Type IIa and Type IIb (Boullier & Bouchez 1978) quartz ribbons composed of strain-free mosaics of the fine grain size. Many ribbons exhibit a slight pinch and swell morphology, in which the thinned areas of the ribbon are in contact with undulatory seams of refractory phases. Undulatory seams of fine-grained Fe-oxides and biotite, similar in form to stylolites, cross-cut both feldspar and quartz grains parallel to the foliation in low to moderately deformed specimens (Fig. 3c). Indented quartz–quartz grain contacts, resembling pressure-solved pebbles in a deformed conglomerate, are also present (Fig. 3d).

Monocrystalline quartz grains and recrystallized mosaics display strong lattice preferred orientations. Quartz *c*-axis patterns are typically asymmetric Type I crossed girdles and asymmetric partial crossed girdles (Bailey & Simpson 1993) indicating a significant component of non-coaxial strain (Schmid & Casey 1986). Quartz *c*-axis maxima occur between 25° and 40° away from the foliation pole and are consistent with basal and rhomb slip in <a> (Schmid & Casey 1986). These asymmetric fabrics, along with asymmetric quartz and mica tails on feldspar porphyroclasts, mica fish, and shear bands, are all consistent with NW-directed thrusting under non-coaxial strain.

STRAIN ANALYSIS

Techniques

Strain analysis in these quartzo-feldspathic crystalline rocks is complicated by the heterogenous nature of strain within and among the individual phases. The different deformation responses of feldspar and quartz call for two independent strain analysis techniques, neither of which defines the bulk-rock strain completely but each of which places limits on the amount and geometry of strain in these rocks. Feldspar deformed by cataclasis, boudinage, and dissolution, therefore measurements of minimum absolute stretch and dilatation are possible. Original igneous quartz grains underwent shape changes through predominantly dislocation glide, thus estimates of the fabric ellipsoid can be made from the aspect ratio of deformed grains. Although dislocation glide was the dominant deformation mechanism in quartz, recrystallization and solution transfer processes were also active. Thus quartz grains shapes cannot be used as strain markers only fabric markers. Two dimensional strain measurements were made on different planes in order to estimate the three dimensional strain geometry. Measurements were made on thin sections cut normal to the foliation and parallel to the lineation (XZ), and normal to both foliation and lineation (YZ).

Feldspar strain estimates

The minimum absolute stretch of feldspar fragments and their associated transverse veins was determined from:

$$S = L_f/\Sigma L_i, \quad (1)$$

where L_f is the total length of the boudinaged feldspar-vein complex and ΣL_i is the summation of feldspar fragment lengths. Ramsay (1967) included an equal number of gap (vein) and fragment measurements in his method for stretch determination using rigid objects. Hossain (1979) showed that a truer estimate of the strain in the matrix surrounding the boudinaged object was achieved by including fibres at either end of the boudin trail in the standard L_f measurement. Ferguson (1981) improved the estimate of matrix strain by using an incremental strain reversal technique applied to the centers of rigid fragments. Measurements were made using both the standard method, including half of each tail at the end of a boudin train, and Ferguson's strain reversal method. Complex feldspar-vein trains have numerous irregular shaped fragments, therefore the strain reversal method was accomplished with the aid of a microcomputer program that restored the fragments in an iterative fashion. Individual feldspar-vein trains generally contain multiple fragments, including many that do not span the total vein thickness (Fig. 4); in these cases up to six parallel measurements were made on each feldspar-vein complex and the mean value used as the estimate of stretch for that boudin train. Another

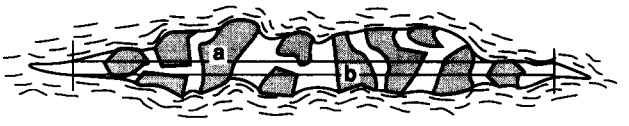

Fig. 4. Boudinaged feldspar-vein complex with multiple fragments not all of which span the entire vein thickness. Feldspar fragments are shaded, quartz is white, and muscovite grains are platy. Two traverses measured to determine the stretch (S).

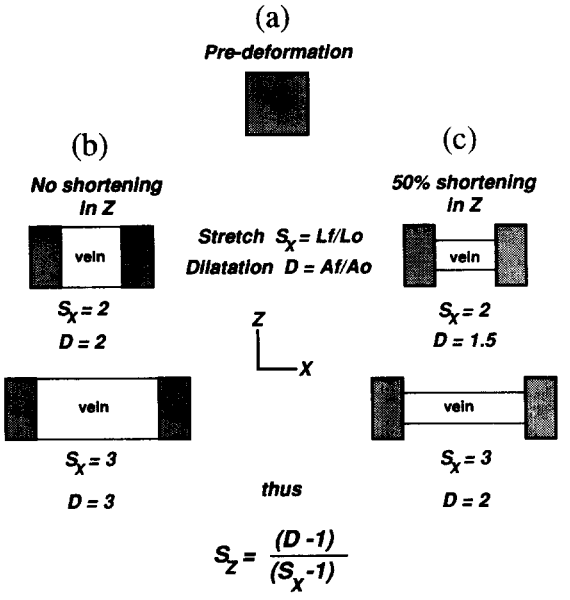

Fig. 5. Schematic diagram illustrating the relationship between stretch, dilatation and amount of shortening in the Z-direction. (a) Undeformed feldspar. (b) With no shortening in Z-direction, stretch and dilatation increase at the same rate. (c) With 50% shortening in Z-direction, the increase in dilatation is less than increase in stretch. For a given amount of stretch and dilatation and the amount of shortening parallel to the Z-direction is given by the equation at the bottom.

estimate of the strain was made by determining the dilatation (D) of boudin trains,

$$D = A_f/\Sigma A_i \quad (2)$$

where A_f is the total area of the boudin train and ΣA_i is the summation of the area of feldspar fragments. Measurements were made on traced images of boudins and transverse veins using a computerized image analysis system.

The amount of shortening normal to the foliation was estimated by combining stretch and dilatation measurements. With no shortening in the Z-direction ($S_Z = 1$), the amount of dilatation would be equal to stretch (Figs. 5a & b). In thin section, the vein that separates fragments would be as thick as the fragments and display no bow-tie geometry. With shortening parallel to the Z-direction ($S_Z < 1$) then dilatation should be less than stretch and with increasing strain the ratio of dilatation to stretch decreases (Figs. 5a & c). In this case the vein would be thinner than the fragment thickness and a bow-tie geometry is expected. Stretch normal to the foliation (S_Z) can be calculated from,

$$S_Z = (D - 1)/(S_X\text{-}1), \quad (3)$$

thus an individual boudin train can yield information about the stretch in both the X-direction (or the Y-direction in YZ sections) and the Z-direction.

The best estimate of shortening in the Z-direction can be made by plotting stretch vs dilatation for the entire population of feldspars from a sample (i.e. all feldspars from thin sections cut perpendicular to both the XZ and YZ planes). The data should fall along a straight line which intersects the origin ($S = 1$, $D = 1$), and whose slope is an estimate of the shortening in the Z-direction (Fig. 6). A feldspar that has not been stretched ($S_X = 1$), will not have been dilatated and the deformation path must, therefore, originate at $S = 1$ and $D = 1$ (Fig. 5a). With no shortening in the Z-direction, stretch equals dilatation and the data would fall along the line with a slope of one (Fig. 6). If shortening has occurred in the Z-direction then dilatation will be less than stretch and the data would plot along a line with a slope less than one (Fig. 6). All measured feldspar stretches from both XZ and YZ sections for a sample were plotted and a best-fit regression technique applied to the data (Fig. 7). The correlation coefficient (r-value) was used to estimate the error that was applied to the X, Y and Z values, which were then combined to yield the X/Y and Y/Z error values.

The population of boudinaged feldspar fragments in any thin section yields a range of stretch and dilatation estimates. Individual feldspars fracture once their yield strength is exceeded. The stage at which a feldspar fractures and how much it extends are determined by the orientation of the crystal lattice as well as by the orientation and magnitude of the applied stress. Some feldspars fail and boudinage early in the deformation; others undergo some rotation before they are suitably oriented to fracture. Feldspars that have been extensively boudinaged display abundant fractures parallel to cleavage planes whereas feldspars that have been slightly boudinaged are fractured along non-rational planes. Even at low to moderate strain some relict feldspars have not boudinaged at all. Feldspars with fractures parallel to cleavage planes have felt the least amount of matrix strain before boudinaging and therefore give the best estimates of stretch for the matrix.

Quartz fabric estimates

Estimates of quartz fabric ellipsoids were made using R_f/ϕ_f strain analysis techniques for elliptical objects. Original quartz grains in the protolith were deformed into elliptical lenses and ribbons in the mylonite. Measurements were made on monocrystalline grains and grains with a core and mantle texture whose outline could be clearly distinguished. Quartz grains were traced from thin sections and the aspect ratio (R_f) and orientation of the long axis (ϕ_f) measured for each grain. The data were plotted on a hyperbolic net and the R_S value determined using De Paor's (1988) technique (Fig. 8). The number of grains measured per section varied between 24 and 156. The validity of the initial R_S value was tested by dividing the data set in half along a series of

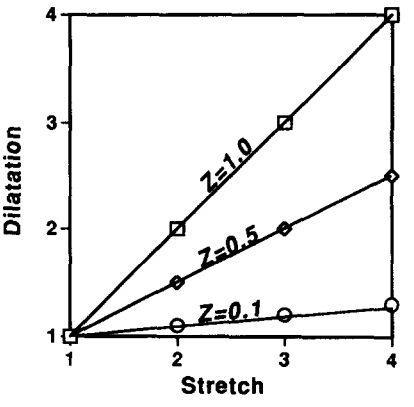

Fig. 6. Schematic dilatation vs stretch plot for ideal populations of boudinaged feldspars. With no shortening in the Z-direction ($Z = 1.0$) the slope of the line equals unity. With 50% shortening in the Z-direction ($Z = 0.5$) the slope of the line equals 0.5. With 90% shortening in the Z-direction ($Z = 0.1$) the slope of the line equals 0.1.

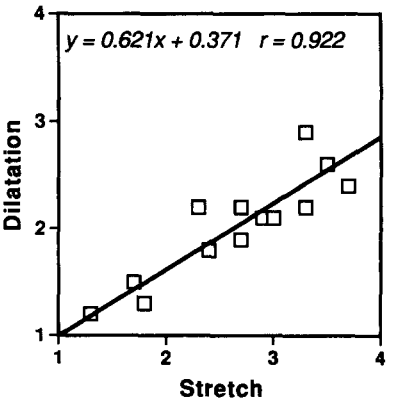

Fig. 7. Dilatation vs stretch plot of boudinaged feldspars from Specimen BR1104. Equation given for best fit line. Slope of the line corresponds to the amount of shortening the Z-direction ($Z = 1.0$). Correlation coefficient is r.

isogons (loci of initial orientation) and the tightness of the intersecting isogons used to estimate the error. A second test using regularly spaced isogons to divide the data into subpopulations was performed to detect any primary fabric in the protolith (Lisle 1977, De Paor 1988). If the rock started with a random fabric then after deformation the subpopulations should contain an equal number of data points. The observed values were compared with those expected for a random initial orientation employing standard chi-square analysis. All samples exceeded the 70% confidence level for an initial random fabric and most samples exceeded the 85% confidence level (Table 1).

Results

Feldspar stretch measurements were performed on nine samples of protomylonites and mylonites (Table 1). The results are plotted on a logarithmic Flinn diagram (Fig. 9). Quartz fabric measurements from 14 samples (Table 1) are also included in Fig. 9. The five samples without feldspar data had grains that were too small to make reliable measurements or had experienced post-deformational saussuritization that obscured original

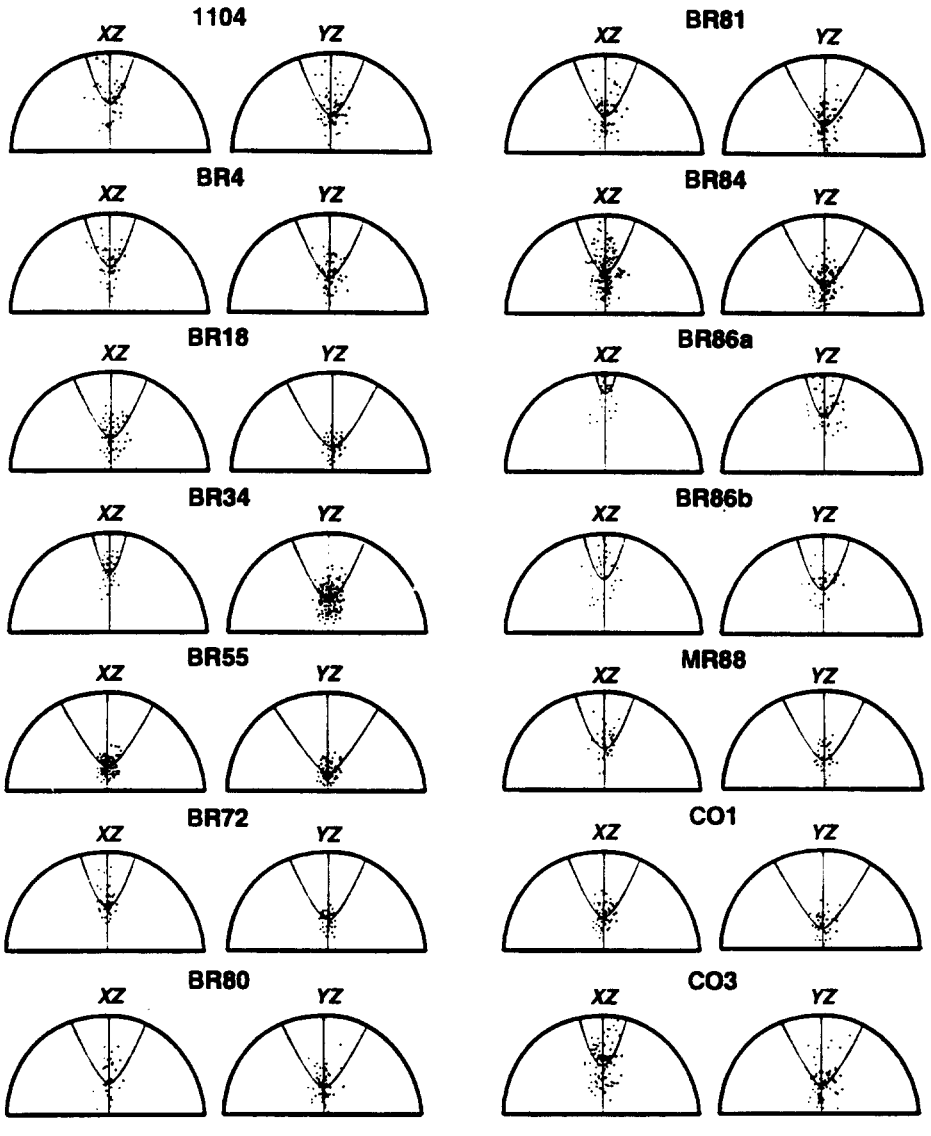

Fig. 8. R_f/ϕ_f plots for quartz data.

grain boundaries. All quartz and feldspar data plot within the field of apparent flattening.

The error for quartz data was typically 10–15% of the X/Y and Y/Z values, or a ±0.1 deviation from the K*-value (The quartz data described the fabric ellipsoid, not the finite strain ellipsoid, so that K* is used rather than K). The error for feldspar data was typically 15–25% of the X/Y and Y/Z values, with the largest errors up to 40%. Feldspar K-values typically had a ±0.3 deviation, with the largest range of K-values for a single sample

Table 1. Quartz and feldspar strain values. K* and K=ln(X/Y)/ln(Y/Z). Values in parentheses are the minimum and maximum K*- or K-values for each sample. Chi-square probabilities of quartz data given as being greater than a certain probability that the data presents a random fabric

	Quartz				Feldspar					
					Standard method			Ferguson method		
Specimen	X/Y	Y/Z	K*	χ^2	X/Y	Y/Z	K	X/Y	Y/Z	K
BR1104	1.4 ± 0.1	2.8 ± 0.2	0.3 (0.2–0.4)	>0.95	1.2 ± 0.2	3.0 ± 0.8	0.1 (0–0.5)	1.2 ± 0.4	4.2 ± 1.3	0.1 (0–0.6)
BR4	1.4 ± 0.1	2.7 ± 0.3	0.3 (0.2–0.4)	>0.75	1.9 ± 0.5	4.0 ± 1.5	0.4 (0.2–0.9)	1.9 ± 0.8	5.8 ± 2.8	0.4 (0.1–0.8)
BR18	1.3 ± 0.1	1.9 ± 0.1	0.7 (0.6–0.8)	>0.80	1.5 ± 0.3	3.6 ± 0.8	0.3 (0.1–0.6)	1.4 ± 0.2	5.2 ± 0.9	0.2 (0.1–0.4)
BR34	2.2 ± 0.2	2.5 ± 0.4	0.8 (0.6–1.1)	>0.90	1.6 ± 0.2	2.3 ± 0.3	0.5 (0.3–0.8)	1.4 ± 0.4	3.2 ± 1.0	0.3 (0–0.8)
BR55	1.2 ± 0.1	1.6 ± 0.2	0.8 (0.6–0.9)	>0.90	1.5 ± 0.2	1.6 ± 0.2	0.9 (0.5–1.6)	1.5 ± 0.2	2.1 ± 0.3	0.5 (0.2–0.9)
BR72	1.4 ± 0.0	2.4 ± 0.1	0.4 (0.3–0.4)	>0.85	1.6 ± 0.3	2.3 ± 0.3	0.5 (0.3–0.9)	1.6 ± 0.6	3.2 ± 1.3	0.4 (0–1.1)
BR80	1.2 ± 0.1	2.1 ± 0.5	0.2 (0.1–0.4)	>0.85						
BR81	1.3 ± 0.1	2.2 ± 0.1	0.3 (0.1–0.4)	>0.70	1.5 ± 0.3	2.5 ± 0.8	0.4 (0.1–0.7)	1.5 ± 0.3	4.5 ± 1.0	0.3 (0.1–0.5)
BR84	1.5 ± 0.2	2.1 ± 0.2	0.5 (0.3–0.8)	>0.90						
BR86a	1.8 ± 0.1	4.8 ± 0.2	0.4 (0.2–0.6)	>0.75	1.5 ± 0.5	3.4 ± 1.3	0.4 (0.1–0.9)	1.6 ± 0.3	7.3 ± 1.4	0.2 (0.1–0.4)
BR86b	1.2 ± 0.1	3.6 ± 1.1	0.1 (0–0.2)	>0.80						
MR88	1.4 ± 0.2	2.2 ± 0.2	0.5 (0.3–0.7)	>0.85	1.5 ± 0.5	2.5 ± 0.7	0.4 (0–1.1)	1.4 ± 0.3	3.0 ± 0.7	0.3 (0.1–0.6)
CO1	1.4 ± 0.1	1.8 ± 0.2	0.6 (0.5–0.8)	>0.75						
CO3	1.9 ± 0.1	2.1 ± 0.1	0.8 (0.6–1.0)	>0.75						

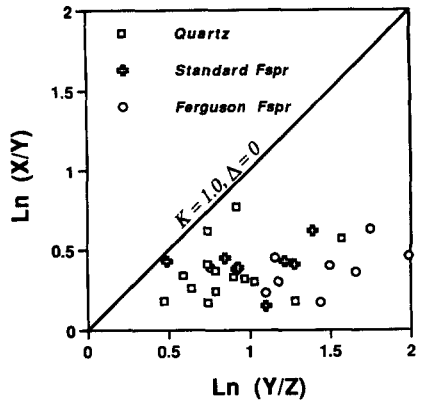

Fig. 9. Logarithmic Flinn diagram of quartz and feldspar strain data for Blue Ridge protomylonites and mylonites. Line of plane strain (K = 1, Δ = 0). All data plot within field of apparent flattening.

between 0 and 1.1 (Table 1). The larger error in the feldspar data relative to the quartz data is caused by the three values (S_X, S_Y, S_Z), rather than the two R_S values for quartz, in which the error estimate was applied. At the high end of the error range, only five samples attained a K- or K*-value of one or greater (Table 1). The strain data and error estimates are plotted for three samples (BR18, BR86a, and CO3) in Fig. 10. The Ferguson method consistently gave larger stretch estimates than the standard method as expected. The Ferguson method also gave higher K-values at low stretches than the standard method, but the two techniques yielded similar results at higher K-values (Table 1).

GEOCHEMICAL ANALYSIS

Whole-rock chemical analyses of major element and selected trace elements for three protolith/mylonite pairs are summarized in Table 2. Each suite of samples comes from a different protolith; the CO1/CO3 protolith a biotite-rich granite, the BR18 protolith a charnockite, and the BR86a protolith a leucocratic granite (Table 3). Specimens CO1/CO3 show few chemical differences between protolith granite and mylonite. In samples BR18 and BR86a SiO_2, Na_2O and K_2O decrease in abundance while TiO_2, MnO and P_2O_5 increase in the mylonite relative to the protolith (Table 2). The concentration of refractory elements (Ti, P, Mn, Y and Zr) in the protolith are plotted against their concentrations in the mylonite (Fig. 11). No enrichment of immobile elements occurred in the mylonite for the CO1/CO3 suite, whereas in BR18 and BR86a these elements are enriched in the mylonite relative to the protolith (Fig. 10 and Table 2). The relative enrichment of refractory elements coincides with a modal increase in sphene, zircon, apatite and epidote in the mylonite relative to the protolith for BR18 and BR86a (Table 3). The bulk density of the protolith and mylonite was calculated from modal data using representative mineral densities (Table 3). Density changes of less than 3% occurred between the protolith and mylonite for all three pairs of samples.

O'Hara (1990) demonstrated that bulk-rock volume change (Δ) may be defined as:

$$C_f/C_i = 1/(1 + \Delta), \quad (4)$$

where C_i and C_f refer to the initial and final concentrations of a chemical species, respectively. This relationship is valid if density changes between protolith and mylonite are small. The slope of the best-fit line from Fig. 10 can be used as the C_f/C_i term in equation (4), and thus the volume loss can be calculated. The best-fit line for the CO1/CO3 suite has a slope of 0.93 (r = 1.0) and corresponds to a 7% volume gain, that for the BR18 suite has a slope of 1.6 (r = 0.9), corresponding to a 38% volume loss, and that for the BR86a suite has a slope of 2.7 (r = 0.9), corresponding to a 63% volume loss (Fig. 11). The slight volume gain recorded for the CO1/CO3 suite serves to emphasize that volume loss cannot be assumed to have occurred in all high strain zones in the Blue Ridge basement rocks.

Protolith and mylonite modal analyses for the BR18 and BR86a suites exhibit significant mineralogic changes (Table 3). The modal abundance of K-feldspar and plagioclase generally decreased in the mylonite relative to its protolith, whereas muscovite, biotite and epidote increased. Quartz either increased in modal abundance or exhibited only minor changes in the deformed rock. CO1/CO3 showed no substantial modal changes between the protolith and mylonite, however modal comparisons from samples without whole-rock geochemical data are generally similar to the BR18 and BR86a suites.

DISCUSSION

Deformation conditions

Feldspar in the mylonitic rocks deformed by cataclasis, with both narrow Mode I extension cracks and trains of boudinaged feldspar fragments separated by transverse veins. We found no evidence for subgrain development, deformation twinning, or recrystallization along grain boundaries or cracks, which suggests that crystal plastic processes were not active and deformation temperatures were well below 450°C (Tullis 1983, Simpson & De Paor 1991). The orientation and geometry of the transverse veins and muscovite selvages parallel to foliation suggest that feldspar dissolution with concurrent reaction to white mica and quartz occurred along foliation planes. The distinct bow-tie geometry is consistent with dissolution of the fibrous quartz precipitated in veins, but could also be accomplished by enhanced strain localization in the recrystallized quartz grains.

The bow-tie shaped transverse veins, feldspar and quartz grains mantled with white mica normal to the foliation, indented quartz grain contacts, and undulatory seams of inert minerals parallel to the foliation suggest that pressure solution was operative. Experimental studies by Rutter (1976, 1983) indicate that pressure solution can be an important deformation mechanism in silicates at temperatures under 400°C.

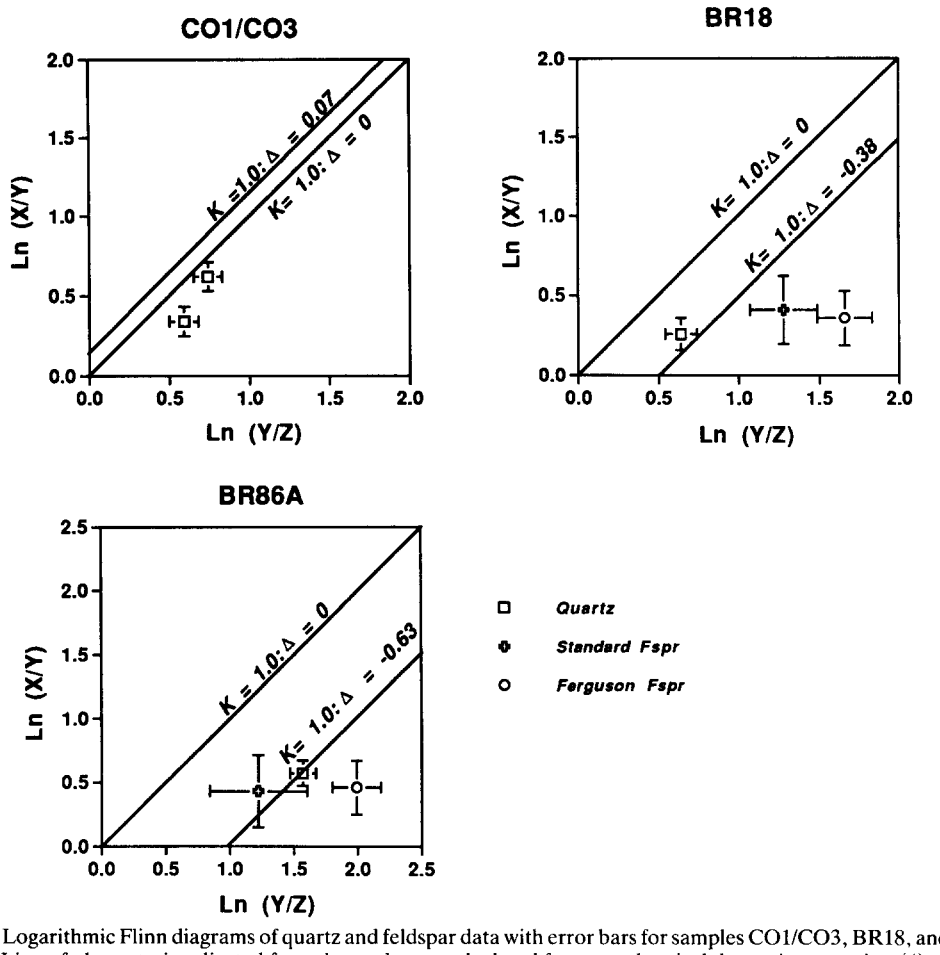

Fig. 10. Logarithmic Flinn diagrams of quartz and feldspar data with error bars for samples CO1/CO3, BR18, and BR86a. Line of plane strain adjusted for volume change calculated from geochemical data using equation (4).

Cataclasis of feldspar would enhance pressure solution by providing more surface area for grain boundary dissolution.

Quartz also deformed by crystal plastic mechanisms. Monocrystalline lenses and ribbons deformed by dislocation glide, but core and mantle textures, deformation bands, and occasional strain-free new grains indicate rotational recrystallization also occurred. Crystal plasticity becomes effective in quartz at temperature near 300°C, whereas the lack of complete recovery suggests

Table 2. Whole-rock chemical analyses of protolith and tectonite for three suites of samples. In weight percent for major elements and ppm for minor elements. Samples analyzed by X-Ray Assay Inc. of Toronto, Canada

	CO1/CO3				BR18		BR86	
	Protolith		Tectonite		Protolith	Tectonite	Protolith	Tectonite
	Mean (N = 3)	S.D.	Mean (N = 3)	S.D.	(N = 1)	(N = 1)	(N = 1)	(N = 1)
SiO_2	62.3	0.5	62.7	0.7	61.6	57.3	73.3	67.3
TiO_2	1.60	0.06	1.50	0.05	1.33	2.08	0.29	0.78
Al_2O_3	13.3	0.4	13.3	0.2	15.9	14.2	13.7	14.0
Fe_2O_3	7.99	0.21	7.89	0.19	6.48	9.85	2.25	4.25
MnO	0.12	0.00	0.12	0.00	0.10	0.14	0.04	0.06
MgO	1.16	0.10	1.14	0.05	1.21	1.66	0.32	0.56
CaO	3.35	0.15	4.25	0.41	2.33	5.40	0.92	2.25
Na_2O	3.04	0.42	3.34	0.01	3.37	2.78	2.95	2.67
K_2O	4.15	0.20	2.87	0.07	5.90	3.15	5.88	5.21
P_2O_5	0.69	0.04	0.63	0.03	0.52	0.98	0.07	0.30
Cr_2O_3	0.03	0.00	0.04	0.00	0.03	0.04	0.05	0.04
LOI	0.85	0.29	1.12	0.09	0.90	0.25	0.50	0.85
Rb	158	10	131	2	181	67	264	173
SR	315	29	416	34	359	538	113	261
Y	89	11	111	9	82	57	10	44
Zr	1123	48	1053	21	1100	820	231	611
Nb	33	11	33	11	22	46	10	30
Ba	1370	115	751	49	2030	1710	519	1440

Table 3. Modal analyses of protolith and mylonites for three suites of samples. Bulk density (ρ) calculated from modal data using representative mineral densities

	BR18		BR86a		CO1/CO3	
	Protolith	Tectonite	Protolith	Tectonite	Protolith	Tectonite
Alkali feldspar	47.5	36.6	39.6	27.2	26.9	24.4
Quartz	27.0	25.0	29.3	32.2	22.5	24.1
Plagioclase	13.2	10.1	18.0	13.0	20.3	18.2
Hypersthene	5.3	—	—	—	—	—
Biotite	4.3	14.5	5.0	10.1	18.9	20.3
Sphene	0.8	1.0	1.1	2.2	1.8	2.2
Muscovite	0.7	7.4	4.4	11.0	5.7	6.9
Epidote	0.6	4.7	2.3	4.0	3.5	3.6
Apatite	0.5	0.5	0.2	0.2	0.2	0.2
Opaque	0.1	0.2	0.1	0.1	0.2	0.1
ρ	2.67	2.72	2.65	2.72	2.74	2.75

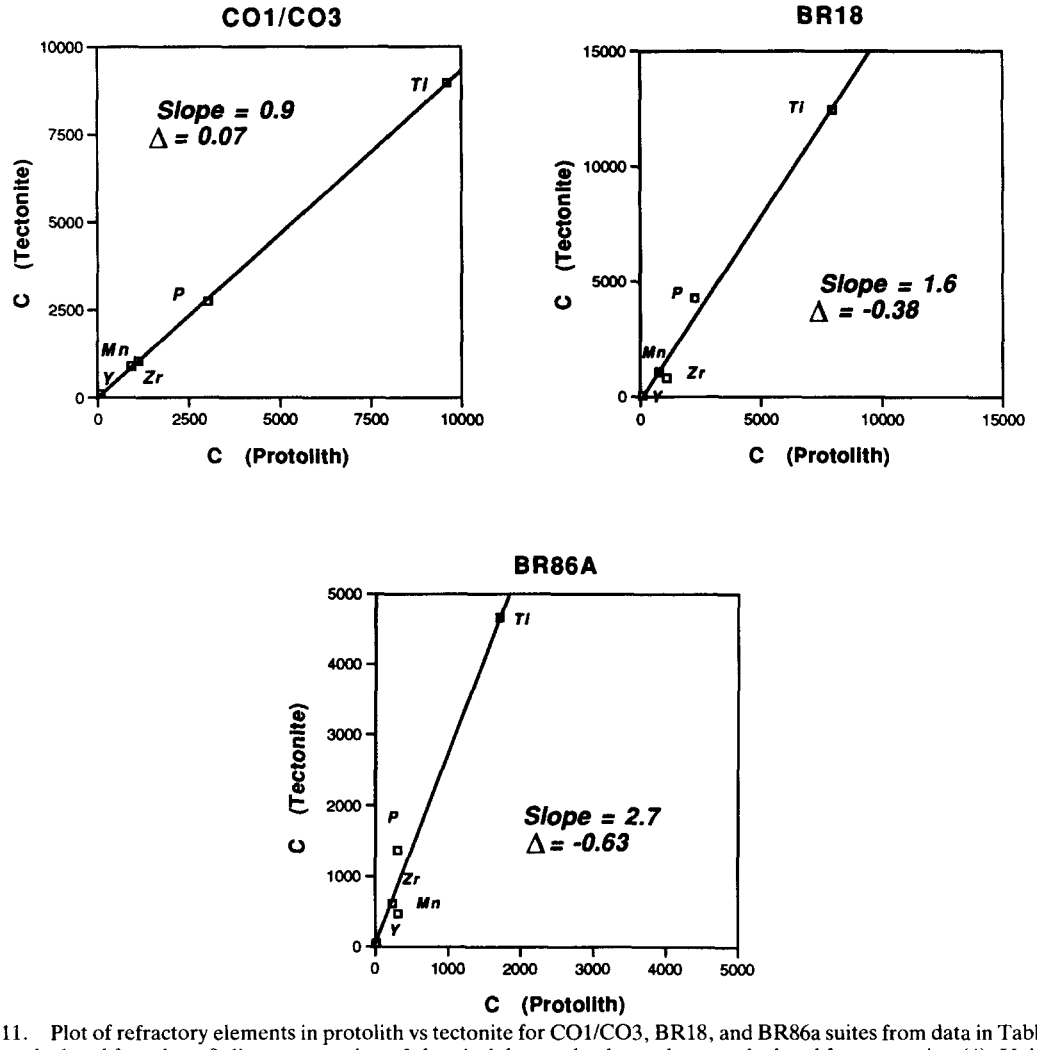

Fig. 11. Plot of refractory elements in protolith vs tectonite for CO1/CO3, BR18, and BR86a suites from data in Table 2. Slope calculated from best-fit linear regression of chemical data and volume change calculated from equation (4). Units in ppm.

deformation temperatures within the greenschist facies (Voll 1976, Simpson 1983). Although both relict quartz and fibrous quartz in veins were deformed through crystal-plastic mechanisms, there are distinct differences in their response to deformation. Original igneous quartz grains underwent large shape changes almost entirely by dislocation glide, as illustrated by monocrystalline quartz ribbons with only minor recrystallization along deformation bands and grain margins. In contrast, quartz precipitated in extension cracks and transverse veins is thoroughly recrystallized, with the exception of quartz in small extension fractures and at the vein-fragment margin.

Dissolution in shear zones

The early stages of solution zone development have been described by Burg & Iglesias Ponce de Leon (1982) in a weakly deformed granite. In the North Carolina Blue Ridge province Boyer (1984), Boyer & Mitra

(1988), and O'Hara (1990) have described solution zones in basement and cover rocks that carry a foliation. We have not observed undulatory seams of insoluble minerals in undeformed basement, but they do occur in rocks that display a weak foliation, fractured feldspars, and slightly flattened lenses of quartz. O'Hara (1990) suggested that the formation of discrete solution zones will result in localized deformation due to reaction of feldspar to phyllosilicates. If solution zones represent the inhomogeneity upon which shear zones nucleate then it seems reasonable that solution zones should occur in unsheared basement rocks. Whether or not they develop into a high strain zone would depend on their orientation and the stress conditions. However, it is not clear to us what mechanism would act to concentrate solution zones rather than leaving many small and dispersed solution surfaces throughout the rock.

The boudinaged feldspars record a substantial local volume increase which may have left temporary voids in the rock, thereby enhancing bulk-rock permeability and facilitating fluid movement. Fracturing of feldspar would also increase the available surface areas for dissolution. The transformation of quartz from equant to elongate lenses would also increase the effective area for pressure solution (i.e. more surface area perpendicular to the Z-direction). In spite of the evidence for extensional strain in both the X- and Y-direction dissolution in the Z-direction must have more than offset the dilatated feldspars, leading to bulk-rock volume loss in some samples.

Quartz veins make up <5% of the total rock volume in both undeformed and deformed basement, however there is far more undeformed rock than mylonite, and it would be possible to offset the large volume loss in mylonites by meager volume gains over large areas. Most, but certainly not all, veins in the shear zones have been deformed in the thrusts, and many can be traced into undeformed regions in massive crystalline rock. If a dispersed network of veins accounts for the volume balance, then a mechanism is needed for first focusing the dissolution in zones and then dispersing the fluids to form veins. Deformation in the basement rocks represents an early period in the NW-directed Appalachian thrusting. The semi-brittle shear zones are both kinematically and temporally related to brittle faults in the cover sequence (Bartholomew 1987). Many of these structurally higher fault zones exhibit dilatational features and may represent a possible sink for the dissolved material from shear zones at depth.

Interpretation of strain data

The apparent flattening strains recorded by the Blue Ridge tectonites could be the result of a true tectonic flattening strain, volume loss during deformation, or a combination of both. If volume loss occurs the line of plane strain on the Flinn diagram is shifted along the abscissa towards the right. The slight volume gain in CO1/CO3 shifts the line of plane strain to the left, and the quartz data records a true tectonic flattening strain (Fig. 10). BR18 experienced 38% volume loss, which places the quartz data near the adjusted line of plane strain, whereas both the standard and Ferguson boudinage analyses give points for feldspar that plot in the field of flattening (Fig. 10). The 63% volume loss in BR86a shifts the line of plane strain well to the right and the quartz data plot along the plane strain line, whereas the standard boudinage analysis yields data that plot slightly in the field of constriction and the Ferguson technique puts them slightly into the field of flattening (Fig. 10). Although some of the data plot near the line of plane strain, feldspars in the YZ sections from all the samples examined are boudinaged and extended ($S_Y > 1$ and $\varepsilon_Y > 0$) indicating that the Blue Ridge mylonites experienced a component of true tectonic flattening strain.

Table 4. S_Z, Δ, K and K′ values for samples with feldspar data. S_Z calculated from slope of dilatation versus stretch for boudinaged feldspars. $\Delta = S_Z - 1$. $K = \ln(X/Y)/\ln(Y/Z)$. $K' = \ln(X/Y)/\ln(Y/Z)'$, where $\ln(Y/Z)' = \ln(Y/Z) + \ln(1 + \Delta)$

Ferguson's method

Specimen	S_Z	Δ	K	K′
BR1104	0.5	−0.5	0.1	0.2
BR4	0.4	−0.6	0.4	0.8
BR18	0.4	−0.6	0.2	0.5
BR34	0.8	−0.2	0.2	0.3
BR55	0.7	−0.3	0.5	1.0
BR72	0.5	−0.5	0.4	1.0
BR81	0.4	−0.6	0.3	0.7
BR86a	0.3	−0.7	0.2	0.6
MR88	0.7	−0.3	0.3	0.5
		Mean	0.3	0.6

Standard method

Specimen	S_Z	Δ	K	K′
BR1104	0.6	−0.4	0.1	0.2
BR4	0.5	−0.5	0.4	0.9
BR18	0.5	−0.5	0.3	0.7
BR34	0.9	−0.1	0.5	0.6
BR55	0.8	−0.2	0.9	1.6
BR72	0.6	−0.4	0.5	1.3
BR81	0.6	−0.4	0.4	0.9
BR86a	0.5	−0.5	0.4	0.8
MR88	0.8	−0.2	0.4	0.6
		Mean	0.4	0.8

Stretch and dilatation measurements from feldspar boudin trains were used to estimate the amount of stretch parallel to the Z-direction, which may be due to tectonic shortening, volume loss, or a combination of the two processes. Chemical evidence indicates that volume loss occurred in some samples. In lieu of chemical data, the value of S_Z may be used as a proxy for volume loss. The S_Z value is a maximum volume loss estimate because it assumes no tectonic shortening occurred parallel to the Z-direction (i.e. all shortening in that direction has occurred due to volume loss alone). For samples with feldspar data the S_Z value was used as an estimate of volume loss. Samples BR18 and BR86a had S_Z values of 0.4 and 0.3 (Ferguson method), which correspond to 60% and 70% volume loss, respectively (Table 4). Chemical evidence indicates that these samples experienced 38% and 63% volume loss, thus

volume loss estimates using shortening values overestimate the true volume loss. S_Z values for all samples with feldspar data ranged from 0.9 to 0.3 (Table 4) indicating volume losses between 10% and 70%. In order to evaluate the nature of the tectonic strain, the line of plane strain was adjusted for volume loss and a tectonic K-value calculated (Table 4 and Fig. 12). Without considering the effects of volume loss, K-values averaged 0.3 using the Ferguson method and 0.4 using the standard method (Table 4). Adjusting for volume loss, K-values increased to a mean value of 0.6 and 0.8, respectively (Table 4). The tectonic K-values are closer to plane strain than the unadjusted values, however nearly 90% of the data fall in the field of flattening ($K < 1$). Furthermore, this technique overestimates the effect of volume loss because all shortening parallel to the Z-direction was attributed to volume loss. Tectonic shortening parallel to the Z-direction should occur in most strain regimes, with the exception of volume expanding strains, and thus it is unrealistic to attribute all shortening to volume loss. No adjustment for volume loss underestimates the tectonic K-values, while using S_Z values for volume loss overestimates the K-values. Taken together they bracket the possible tectonic strain geometries.

All of the mylonites from the central and northern Virginia Blue Ridge that we have studied in detail display flattening strains. We have not observed L-tectonites in the Blue Ridge basement, and many of the mylonites have no discernible mineral stretching lineation ($S > L$). We therefore suggest that flattening strains may be penetrative throughout a large region of the basement. Mitra (1979) noted apparent flattening strains in basement rocks from the northern Virginia Blue Ridge. However, penetratively deformed carbonates of the Valley and Ridge province exhibit a large variation in strain geometry (Cloos 1971). The majority of Cloos' strain data plot within the field of apparent flattening, but apparent constrictional strains also occur. Woodward *et al.* (1986) and Evans & Dunne (1991) report predominantly plane strain fabrics from the sedimentary rocks in the same region. The Blue Ridge is the hinterland portion of a series of imbricate thrusts that transported material towards the Appalachian foreland, and basement shear zones comprise an imbricate array of fault zones which stacked the basement (Bailey & Simpson 1993). A possible explanation for the development of regional flattening strains may stem from the deformation sequence which stacks thrust sheets and thereby increases the load on the lowermost thrust sheets (i.e. the Blue Ridge basement sheets). Material is not only transported towards the foreland, but expands laterally, perpendicular to the transport direction.

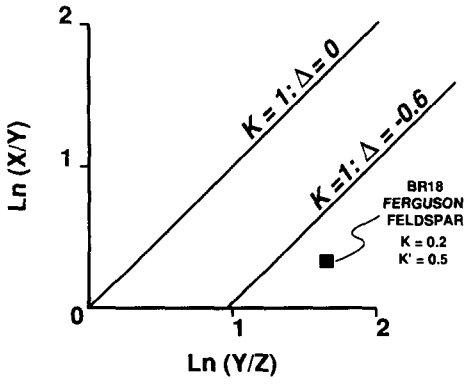

Fig. 12. Logarithmic Flinn diagram of feldspar data for Specimen BR18 with line of plane strain adjusted for volume loss ($K = 1.0$: $\Delta = -0.4$). Without considering volume loss, K-value = 0.2 [$K = \ln(X/Y)/\ln(Y/Z)$]. Adjusting for volume loss, K'-value = 0.5 [$K' = \ln(X/Y)\text{Ln}(Y/Z)'$, where $\ln(Y/Z)' = \ln(Y/Z) + \ln(1 + \Delta)$].

CONCLUSIONS

Deformation in shear zones developed in granitic rocks of the Virginia Blue Ridge occurred under greenschist facies conditions. Feldspar deformed by cataclasis while quartz deformed by crystal plastic mechanisms. The semi-brittle nature of the deformation facilitated significant amounts of dissolution in feldspar and quartz. An enrichment in 'immobile' elements in the tectonites relative to the protolith is interpreted to be caused by bulk volume loss during deformation. However, chemical evidence indicates that not all samples experienced volume loss. Strain measurements on boudinaged feldspars and lensoidal quartz grains plot within the field of apparent flattening of a Flinn diagram. Even considering volume loss, the strain data indicate that shear zones throughout the Blue Ridge experienced true tectonic flattening strains.

Acknowledgements—Financial support for this study was provided by National Science Foundation grants EAR-8816899 and EAR-8916354 to C. Simpson and a Geological Society of America grant and a David Elliott Memorial Field Grant from the Department of Earth and Planetary Sciences at the Johns Hopkins University to C. Bailey. We are grateful to Gulzar Aziz, Greg Dipple, Bob Gower, Mortiz Heimpel, Ken McCaffrey and Dick Tollo for helpful discussions about the subject.

REFERENCES

Bailey, C. M. & Simpson, C. 1993. Extensional and contractional deformation in the Blue Ridge Province, Virginia. *Bull. geol. Soc. Am.* **105**, 411–422.

Bartholomew, M. J. 1987. Structural evolution of the Pulaski thrust system, southwestern Virginia. *Bull. geol. Soc. Am.* **99**, 491–510.

Berthé, D. Choukroune, P. & Jegouzo, P. 1979. Orthogneiss, mylonite and non-coaxial deformation of granite: the example of the South Armorican shear zone. *J. Struct. Geol.* **1**, 31–42.

Boullier, A.-M. & Bouchez, J.-L. 1978. Le quartz en rubans dans les mylonites. *Bull. Soc. geol. Fr.* **7**, 253–262.

Boyer, S. E. 1984. Origin and significance of compositional layering in Late Precambrian sediments, Blue Ridge Province, North Carolina, U.S.A. *J. Struct. Geol.* **6**, 121–133.

Boyer, S. C. & Elliott, D. 1982. Thrust systems. *Bull. Am. Ass. Petrol. Geol.* **66**, 1196–1230.

Boyer, S. C. & Mitra, G. 1988. Relations between deformation of crystalline basement and sedimentary cover at the basement/cover transition zone of the Appalachian Blue Ridge Province. In *Geometries and Mechanisms of Thrusting* (edited by Mitra, G. & Wojtal, S.). *Spec. Pap. geol. Soc. Am.* **222**, 119–136.

Burg, J. P. & Iglesias Ponce de Leon, M. 1985. Pressure-solution structures in a granite. *J. Struct. Geol.* **7**, 341–436.

Cloos, E. 1947. Oolite deformation in the South Mountain fold, Maryland. *Bull. geol. Soc. Am.* **58**, 843–918.

Cloos, E. 1971. *Microtectonics Along The Western Edge Of The Blue Ridge, Maryland and Virginia.* Johns Hopkins University Press, Baltimore.

Coward, M. P. 1976. Strain within ductile shear zones. *Tectonophysics* **34**, 181–197.

Dahlstrom, C. D. A. 1969. Balanced cross-sections. *Can. J. Earth Sci.* **6**, 743–747.

Davis, G. H. 1980. Structural characteristics of metamorphic core complexes, southern Arizona. *Mem. geol. Soc. Am.* **153**, 35–78.

De Paor, D. G. 1988. R_f/ϕ_f strain analysis using an orientation net. *J. Struct. Geol.* **10**, 323–333.

De Paor, D. G., Simpson, C., Bailey, C., McCaffrey, K. J. W., Beam, E., Gower, R. J. W. & Aziz, G. 1991. The role of solution in the formation of boudinage and transverse veins in carbonates at Rheems, Pennsylvania. *Bull. geol. Soc. Am.* **103**, 1552–1563.

Evans, M. A. 1989. Structural geometry and evolution of foreland thrust systems, northern Virginia. *Bull. geol. Soc. Am.* **101**, 339–354.

Evans, M. A. & Dunne, W. M. 1991. Strain factorization and partitioning in the North Mountain thrust sheet, central Appalachians, U.S.A. *J. Struct. Geol.* **13**, 21–35.

Ferguson, C. C. 1981. A strain reversal method for estimating extensions of fragmented rigid particles. *Tectonophysics* **79**, T43–52.

Hanmer, S. & Passchier, C. W. 1992. Shear sense indicators: a review. *Geol. Surv. Pap. Can.* **90**, 17.

Harris, L. D., de Witt, W., Jr. & Bayer, K. C. 1982. Interpretative seismic profile along Interstate I-64 from the Valley and Ridge to the coastal plain in central Virginia. U.S. Geol. Surv., Oil and Gas Investigations, Chart OC-123.

Herz, N. & Force, E. R. 1987. Geology and mineral deposits of the Roseland district and central Virginia. *Prof. Pap. U.S. geol. Surv.* **1371**.

Holmquist, P. J. 1931. On the relations of "boudinage-structure". *Geol. For. Stockholm* **53**, 193–208.

Hossain, K. M. 1979. Determination of strain from stretched belemnites. *Tectonophysics* **60**, 279–288.

Lisle, R. J. 1977. Estimation of tectonic strain ratio from the mean shape of deformed elliptical markers. *Geologie Mijnb.* **56**, 140–144.

Lister, G. S. & Snoke, A. W. 1984. *S–C* mylonites. *J. Struct. Geol.* **6**, 617–638.

Mitra, G. 1979. Ductile deformation zones in Blue Ridge basement rocks and estimation of finite strain. *Bull. geol. Soc. Am.* **90**, 935–951.

O'Hara, K. 1990. State of strain in mylonites from the southern Appalachians, western Blue Ridge province: the role of volume loss. *J. Struct. Geol.* **12**, 419–430.

Ramsay, J. G. 1967. *Folding and Fracturing of Rocks.* McGraw-Hill, New York.

Ramsay, J. G. & Wood, D. S. 1973. The geometric effects of volume change during deformation processes. *Tectonophysics* **16**, 263–277.

Ramsay, J. G. & Huber, M. I. 1983. *The Techniques of Modern Structural Geology.* Academic Press, London.

Rankin, D. W. 1975. The continental margin of eastern North America in the southern Appalachians: the opening and closing of the proto-Atlantic Ocean. *Am. J. Sci.* **275-A**, 298–336.

Rankin, D. W., Drake, A. A., Glover, L., Goldsmith, R., Hall, L. M., Murray, D. P., Ratcliffe, N. M., Read, J. F., Secor, D. T. & Stanley, R. S. 1989. Pre-orogenic terranes. *Geol. Soc. Am. Decade N. Am. Geol.* **F-2**, 7–100.

Rutter, E. H. 1976. The kinetics of rock deformation by pressure solution. *Phil. Trans. R. Soc. Lond.* **A283**, 203–219.

Rutter, E. H. 1983. Pressure solution in nature, theory, and experiment. *J. geol. Soc. Lond.* **140**, 725–740.

Sanderson, D. J. 1976. The superposition of compaction and plane strain. *Tectonophysics* **30**, 35–54.

Schmid, S. M. & Casey, M. 1986. Complete fabric analysis of some commonly observed quartz c-axis patterns. In: *Mineral and Rock Deformation: Laboratory Studies (Paterson Volume)* (edited by Hobbs, B. E. and Heard, H. C.). *Am. Geophys. Un. Monograph Series* **36**, 263–286.

Simpson, C. 1983. Displacement and strain patterns from naturally occurring shear zone terminations. *J. Struct. Geol.* **5**, 597–606.

Simpson, C. & Kalaghan, T. 1989. Late Precambrian crustal extension preserved in the Fries fault zone mylonites, southern Appalachians. *Geology* **17**, 148–151.

Simpson, C. & De Paor, D. P. 1991. Deformation and kinematics of high strain zones. *Geol. Soc. Am. Short Course*, San Diego.

Sinha, A. K. & Bartholomew, M. J. 1984. Evolution of the Grenville terrane in the central Virginia Appalachians. In: *The Grenville Event in the Appalachians And Other Related Topics* (edited by Bartholomew, M. J., Force, E. R., Sinha, A. K. & Herz, N.). *Spec. Pap. geol. Soc. of Am.* **194**, 175–186.

Tollo, R. P. & Aleinokoff, J. N. 1992. The Robertson River igneous suite, Virginia Blue Ridge: a case study in multiple-stage magmatism associated with the early stages of Iapetan rifting. *Geol. Soc. Am. Abs. w. Prog.* **24-2**, 70.

Tullis, J. 1983. Deformation of feldspars. In: *Feldspar Mineralogy, Volume* 2 (edited by Ribbe, H. P.). *Miner. Soc. Am.* 297–323.

Voll, G. 1976. Recrystallization of quartz, biotite, and feldspars from Erstfeld to the Leventian Nappe, Swiss Alps and its geological significance. *Schweiz. miner. petrogr. Mitt.* **56**, 641–647.

Woodward, N. B., Gray, D. R. & Spears, D. B. 1986. Including strain data in balanced cross-sections. *J. Struct. Geol.* **8**, 313–324.